Journal of Materials Chemistry B



PAPER

View Article Online



Cite this: J. Mater. Chem. B, 2025, **13**, 10576

Received 5th June 2025. Accepted 23rd July 2025

DOI: 10.1039/d5tb01345c

rsc.li/materials-b

A dual-targeting photosensitizer for simultaneous mitochondrial and lysosomal disruption in cancer and antibacterial photodynamic therapy†

Chaewoon Cho, ac K. M. K. Swamy, Bingging Sun, Gyoungmi Kim, Lei Liu, +b

Mitochondria and lysosomes are key organelles involved in cell survival and death. Mitochondria regulate energy production, reactive oxygen species (ROS) levels, and apoptosis, while lysosomes manage waste degradation and also play a role in cell death through enzyme release when damaged. Cancer cells often contain more active lysosomal enzymes, making them more vulnerable to lysosome-related cell death. Targeting these organelles with photosensitizers (PSs) in photodynamic therapy (PDT) can achieve enhanced anticancer effects. Dual-targeting PSs, especially those that affect both mitochondria and lysosomes, are rare but highly promising. By simultaneously damaging both organelles, such PSs may trigger stronger therapeutic responses. In this study, we present a novel dual-targeting photosensitizer, MCQ-1, which localizes to both mitochondria and lysosomes and serves as an efficient type I PS for cancer cell treatment. Additionally, MCQ-1 demonstrates remarkable antibacterial activity against Grampositive bacteria, including Staphylococcus aureus (S. aureus) and methicillin-resistant S. aureus (MRSA), under white LFD irradiation

Introduction

Photodynamic therapy (PDT) has emerged as a promising noninvasive therapeutic strategy, which employs photoactivatable agents to selectively eliminate pathological cells. PDT utilizes photosensitizers (PSs) that, upon irradiation with light of an appropriate wavelength, generate reactive oxygen species (ROS), thereby inducing oxidative damage and subsequent apoptosis or necrosis in target cells.²⁻⁷ This strategy has demonstrated substantial potential in the treatment of malignant tumors and infectious diseases, owing to its spatiotemporal controllability, minimal invasiveness, and ability to overcome multidrug resistance.2-7

The development of organelle-specific phototherapeutic agents has emerged as a critical priority for enhancing the selectivity and efficacy of cancer treatment.8 Mitochondria, as key regulators of bioenergetics, redox balance, and apoptotic pathways, represent highly attractive subcellular targets. 9-14

Recent insights into organelle crosstalk have underscored the functional interplay between mitochondria and lysosomes, which cooperatively regulate key metabolic pathways, such as lipid catabolism and glucose homeostasis, via lysosomal hydrolases. 15-17 This bidirectional regulatory mechanism offers a compelling rationale for dual-organelle targeting. By concurrently disrupting lysosomal integrity (thereby impairing autophagic flux and lysosome-dependent mitochondrial quality control) and inducing mitochondrial dysfunctions, dual-targeting strategies potentiate oxidative stress and induce an energy crisis within cancer cells, significantly improving therapeutic outcomes. Nonetheless, only a few examples of mitochondria and lysosome dualtargeting systems have been reported to date. 18-21

On the other hand, bacterial and fungal infections remain a major global health concern, often leading to high mortality rates. Pathogenic bacteria are linked to various diseases, including skin infections, sepsis, and bacteremia, and may even cause cancer through chronic inflammation or the release of carcinogenic metabolites.²² The global rise of antibiotic resistance, driven by the overuse and misuse of antibiotics, has exacerbated this issue, leading to multidrug-resistant "superbugs." These pathogens are now responsible for over 700 000 deaths annually. 23,24 The growing threat of resistant bacteria highlights the urgent need for novel antimicrobial therapies that can overcome the limitations of conventional antibiotics.

^a Department of Chemistry and Nanoscience, Ewha Womans University, Seoul 03760, Korea. E-mail: jyoon@ewha.ac.kr

^b College of Resource and Environment, Anhui Science and Technology University, Fengyang 233100, China. E-mail: liulei@feipan.org

^c Graduate Program in Innovative Biomaterials Convergence, Ewha Womans University, Seoul 03760, Korea

[†] Electronic supplementary information (ESI) available. See DOI: https://doi.org/

Herein, we report a new PS, MCQ-1, which localizes to both mitochondria and lysosomes and serves as an efficient type I PS for cancer cell treatment. Additionally, MCO-1 demonstrates remarkable antibacterial activity against Gram-positive bacteria, including Staphylococcus aureus (S. aureus) and methicillinresistant S. aureus (MRSA), under white LED irradiation.

Results and discussion

Design and synthesis of MCQ-1

For the synthesis of MCQ-1, 9-(4-morpholinobutyl)-9H-carbazole-3carbaldehyde (2) was first prepared following a previously reported procedure. 30-32 Further reaction of 2 with 1,4-dimethylquinolin-1ium iodide in the presence of piperidine afforded MCQ-1 in 50.7% yield (Scheme 1). MCQ-1 was fully characterized using ¹H and ¹³C NMR spectroscopy as well as high-resolution mass spectroscopy (ESI-HRMS) (Fig. S1-S5, ESI†). MCQ-1 exhibited a donor-acceptor (D-A) structure, with carbazole as the electron donor and quinolinium iodide as the electron acceptor, leading to strong intramolecular charge transfer (ICT); this structure resulted in intense fluorescence and facilitated ROS generation. Additionally, its positive charge and the presence of morpholine enabled dualtargeting of mitochondria and lysosomes.

Photophysical properties of MCO-1

First, to investigate the photophysical properties of MCQ-1, UVvis absorption and fluorescence spectra were obtained in various solvents (Fig. 1A and B). In an ACN/PBS solution (5:95, v/v), MCQ-1 showed the highest absorption peak at

Scheme 1 Synthesis of MCQ-1

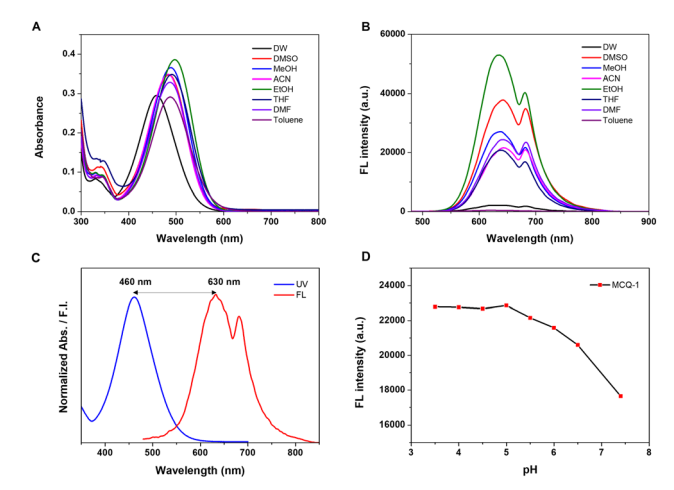


Fig. 1 (A) UV-vis absorption and (B) fluorescence spectra of MCQ-1 (10 μ M) in different solvents; λ_{ex} = 460 nm. (C) Normalized absorption and emission spectra of MCQ-1 (10 μ M) in ACN/PBS solution (5:95, v/v). (D) Fluorescence spectra of MCQ-1 (10 µM) at different pH values: the inset shows the corresponding intensities at 630 nm

460 nm and displayed strong red fluorescence in the 600-700 nm region, with the maximum fluorescence emission observed at 630 nm (Fig. 1C). The large Stokes shift (170 nm) of MCQ-1, with a wide gap between the excitation and emission peaks, reduces self-absorption, making this PS highly suitable for fluorescence imaging.

Next, we examined the fluorescence spectra of MCQ-1 under various pH conditions. Strong fluorescence was observed under acidic conditions (pH 3.5-5.0), but the fluorescence decreased as the pH increased from 5.5 to 7.4 (Fig. 1D). This is attributed to the photoinduced electron transfer (PET) effect from the nitrogen atom in the morpholine structure. However, no significant fluorescence quenching was observed at pH 7.4, indicating that MCQ-1 can serve as a fluorescent probe in biological environments. On the other hand, under acidic conditions, the nitrogen atom in the morpholine structure, which possesses a lone pair of electrons, is readily protonated. This protonation suppresses the PET process, resulting in strong fluorescence.39

ROS generation of MCQ-1

To investigate the photodynamic effect of MCQ-1, we examined its ROS generation ability. First, to evaluate the total ROS generation, fluorescence spectra were measured at different light irradiation times, using 2',7'-dichlorofluorescein diacetate (DCFH-DA) as the indicator. MCQ-1 (10 μM) in PBS buffer solution was irradiated with white LED light (50 mW cm⁻²) for 10 s each time, from 0 to 90 s. The fluorescence peak intensity of DCFH-DA at 520 nm increased with increasing irradiation time (Fig. S6A and B, ESI†). This confirmed the ROS generation of MCQ-1 when activated by light irradiation. Additionally, hydroxyphenyl fluorescein (HPF) was used under the same experimental conditions to detect the hydroxyl radical (*OH) generation. As a result, the fluorescence peak of HPF at 512 nm increased with increasing irradiation time (Fig. S6C and D, ESI†), indicating that MCQ-1 generates ·OH upon light

exposure. Solutions containing only DCFH-DA and HPF were used as controls, and neither showed a fluorescence increase under light irradiation. In contrast, no significant fluorescence changes were observed when ABDA and DHE were used to detect singlet oxygen (1O2) and a superoxide radical anion $(O_2^{\bullet-})$, respectively, under the same conditions, indicating that MCQ-1 does not generate ${}^{1}O_{2}$ or $O_{2}^{\bullet-}$ upon light irradiation (Fig. S7, ESI†). These experiments confirmed that MCQ-1 acts as a PS capable of generating ROS through a type I mechanism, potentially causing the death of cancer cells or bacteria.

Theoretical calculations

The type I PS behavior of MCQ-1 was further elucidated using density functional theory (DFT) and time-dependent density functional theory (TDDFT) calculations. Fig. 2A and B indicate that the HOMO and LUMO are well-separated spatially, indicating that the sensor exhibits ICT characteristics during the $S_0 \rightarrow S_1$ excitation. The electron-hole distribution was then analyzed, as shown in Fig. 2C and D. An equivalent of 0.37 electrons transfers from the carbazole to the quinolone moiety, with a separation distance of 5.37 Å. This denotes a very strong ICT, in terms of both the transfer number and the transfer distance. According to Tang et al.'s theory, 33,34 a strong ICT will boost the ROS production by minimizing the energy difference between singlet and triplet states ($\Delta E_{\rm ST}$), which improves the triplet excited state yield. The calculated energy differences between the singlet and triplet states of MCQ-1 are shown in Fig. 2E (Table S1, ESI†). As expected, the $\Delta E_{\rm S1T2}$ value is only 0.15 eV, which is likely to facilitate the singlet/ triplet ISC process and make MCQ-1 a type I PS.

In vitro PDT effect

Next, the biocompatibility and PDT effect of MCQ-1 were evaluated in vitro using the methyl thiazolyl tetrazolium (MTT) assay in HeLa cells. Under dark conditions, MCQ-1 exhibited low cytotoxicity, maintaining a cell viability greater than 90% even at a concentration of 15 µM. In contrast, under light irradiation, the cell viability decreased sharply with increasing MCQ-1 concentration (Fig. 3). During the same 10-min white LED irradiation treatment, a higher light intensity (0.5 W cm⁻²) resulted in a greater cancer cell death rate compared to that observed at 0.3 W cm⁻², indicating that stronger light led to

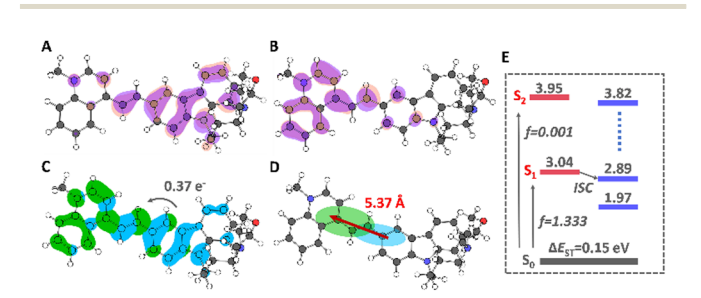


Fig. 2 (A) HOMO; (B) LUMO; (C) electron-hole distribution for the S_0-S_1 excitation process; (D) electron-hole separation; (E) energy level distribution of singlet and triplet states. Green and cvan surfaces represent electron and hole distributions, respectively; f represents the oscillator strength for the excitation process.

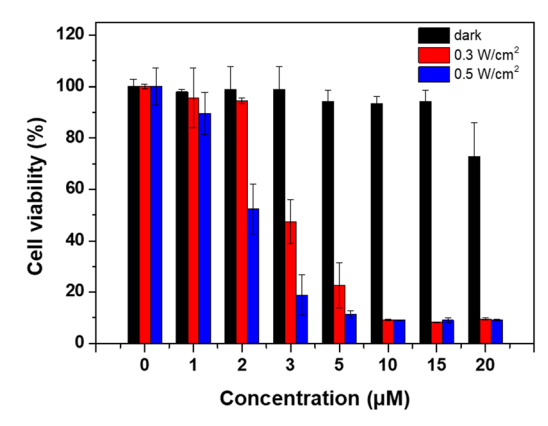


Fig. 3 Cell viability of HeLa cells after MCQ-1 (1-20 μ M) treatment with and without white LED irradiation (0.3, 0.5 W cm⁻², 10 min).

enhanced phototoxicity. Overall, these results confirmed that MCQ-1 exhibits high biocompatibility in the dark along with strong PDT efficiency under light irradiation, demonstrating its potential as an effective PS for cancer treatment.

Mitochondria and lysosome staining

To confirm the dual-targeting ability of MCO-1 toward mitochondria and lysosomes, colocalization experiments were conducted using MitoTracker Blue and LysoTracker Deep Red as fluorescent probes. Colocalization fluorescence images were obtained using confocal laser scanning microscopy (CLSM). HeLa cells were co-stained with MCQ-1 (5 μM, 30 min) and MitoTracker Blue (0.5 μM, 10 min); this was followed by CLSM imaging, which revealed clear colocalization, with a Pearson correlation coefficient (PCC) of 0.84 (Fig. 4A). Similarly, colocalization experiments with LysoTracker Deep Red showed a high PCC value of 0.95 (Fig. 4B). These results confirmed that MCQ-1 enables the simultaneous imaging of mitochondria and lysosomes in live cancer cells.

In vitro fluorescence imaging and antibacterial tests

PDT is also considered a promising antimicrobial strategy, owing to its ability to eliminate multidrug-resistant bacteria

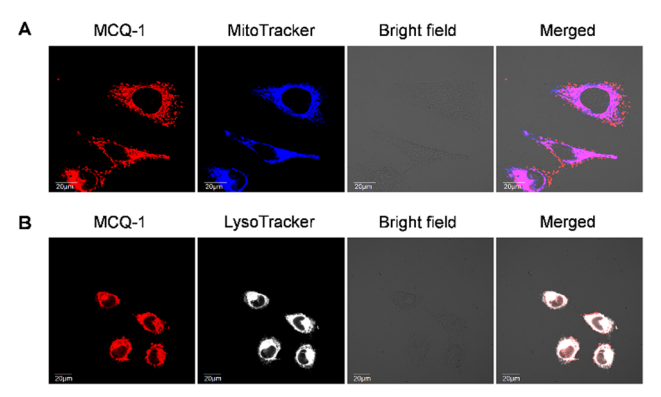


Fig. 4 CLSM images of HeLa cells incubated with MCQ-1 (5 μM, 30 min) and (A) MitoTracker Blue (0.5 µM, 10 min) or (B) LysoTracker Deep Red (5 μM, 10 min).

This journal is © The Royal Society of Chemistry 2025

through ROS generation under light irradiation, without causing side effects such as the development of antibiotic resistance. Therefore, further tests were performed to evaluate the antibacterial PDT effect of MCQ-1. Bacterial experiments were conducted using Gram-positive bacteria, including S. aureus and MRSA, as well as Gram-negative bacteria, including Escherichia coli O157:H7 (E. coli) and extended-spectrum betalactamase producing E. coli (ESBL E. coli).

First, the in vitro bacterial fluorescence images of MCQ-1 were examined using CLSM. When bacteria were treated with MCQ-1 (1 μ M) for 0, 30, and 60 min, Gram-positive strains (S. aureus and MRSA) were rapidly stained, emitting red fluorescence (Fig. 5A and B). Notably, S. aureus exhibited immediate staining upon MCQ-1 treatment. In contrast, Gram-negative strains (E. coli and ESBL E. coli) showed only weak fluorescence after 30 min of incubation with MCQ-1, and only partial staining was observed even after 60 min (Fig. 5C and D). These results indicated that MCQ-1 exhibits superior activity against Gram-positive bacteria, demonstrating its selective targeting of these strains. This selectivity is likely due to the positive charge of MCQ-1, which interacts with the negatively charged thick peptidoglycan layer of Gram-positive bacteria. In contrast, Gram-negative bacteria have a relatively thin peptidoglycan layer and an additional LPS-containing outer membrane, which may hinder the MCQ-1 binding.

Next, the antibacterial effect of MCQ-1 was evaluated using LB agar plates. Gram-positive (S. aureus and MRSA) and Gramnegative (E. coli and ESBL E. coli) strains were pretreated with MCQ-1 at concentrations of 0, 1, 3, 5, and 10 μM, followed by white LED irradiation (50 mW cm⁻², 10 min). As a result, a significantly reduced number of bacterial colonies was observed on the irradiated plates, compared to that on the non-irradiated control plates. Interestingly, as expected from the CLSM experiments, the antibacterial effect was more pronounced on Gram-positive than Gram-negative bacteria (Fig. 6A-D). In Gram-positive bacteria, not only S. aureus but

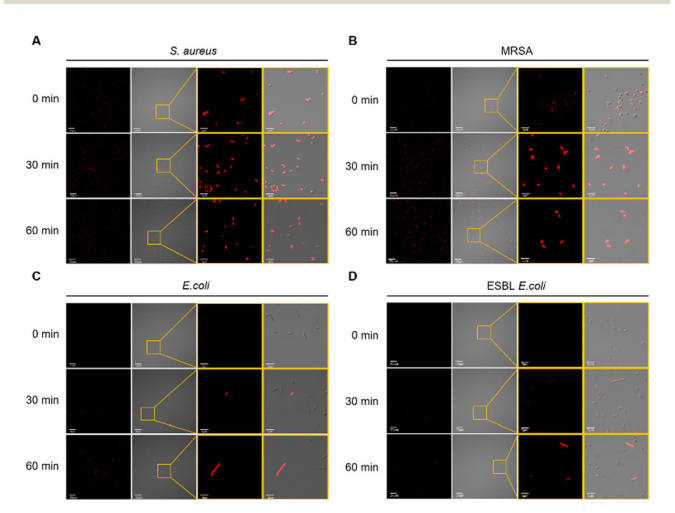


Fig. 5 CLSM images of (A) S. aureus, (B) MRSA, (C) E. coli, and (D) ESBL E. coli treated with MCQ-1 (1 μM) with different incubation times (0, 30, and 60 min).

also the antibiotic-resistant MRSA were mostly eliminated at a low MCQ-1 concentration of 3 μ M, and complete bacterial elimination was observed at 5 µM. However, some residual E. coli and ESBL E. coli bacterial colonies remained even after treatment with 10 µM MCQ-1.

Finally, scanning electron microscopy (SEM) was used to examine morphological changes in bacteria following MCQ-1 treatment with light irradiation. In the case of Gram-positive bacteria, the control group treated only with MCQ-1 (without light exposure) showed smooth and round bacterial surfaces, without cell membrane damage. In contrast, bacteria treated with MCQ-1 followed by white LED irradiation (50 mW cm⁻², 10 min) exhibited perforated cell membranes, along with shrinkage and deformation. Moreover, both E. coli and ESBL E. coli maintained intact surfaces under dark conditions, similar to Gram-positive bacteria. A small number of Gramnegative bacteria with damaged membranes were observed upon light irradiation; however, their number was significantly lower compared to that found for the Gram-positive group (Fig. 6E). These results confirm the antibacterial PDT effect of MCQ-1, which can selectively kill Gram-positive bacteria under light irradiation.

Experimental

Materials and instruments

¹H NMR and ¹³C NMR spectra were recorded using AVANCE III 300 (Bruker) and JNM-EECZ500R (JEOL) spectrometers, respectively. The ESI-HRMS measurement was conducted using a Synapt G2-HDMS mass spectrometer at the Korea Basic Science Institute. Fluorescence emission and UV-vis absorption spectra were measured using a FS-2 fluorescence spectrophotometer (Scinco) and a V-770 UV-Visible/NIR Spectrophotometer (JASco), respectively. CLSM measurements were performed using Olympus Fluoview 3000 and 1200 instruments for colocalization and bacterial imaging, respectively.

Synthesis of 130

9-(4-Bromobutyl)-9H-carbazole (4 g, 13.23 mmol, 1 eq), morpholine (2.3 g, 26.47 mmol, 2 eq) and dry K_2CO_3 (3.66 g, 2 eq) were stirred together in 50 mL of dry acetonitrile overnight. Then, the reaction mixture was filtered, the solvents were evaporated, and the resulting product was purified by column chromatography using a dichloromethane/methanol mixture (95:5, v/v) as the eluent, to obtain compound 1 as a colorless viscous liquid in 98% yield. ¹H NMR (300 MHz, chloroform-d) δ 8.12 (d, 2H), 7.51-7.44 (m, 4H), 7.25 (dd, 2H), 4.34 (t, 2H), 3.69 (t, 4H), 2.35 (m, 6H), 1.93 (tt, 2H), 1.58 (tt, 2H).

Synthesis of 2^{31,32}

A mixture of DMF (1.26 mL, 16.2 mmol, 5 eq) and POCl₃ (1.21 mL, 13.0 mmol, 4 eq) was stirred in an ice bath for 0.5 h, and compound 1 (1 g, 3.24 mmol, 1 eq) dissolved in 1,2-dichloroethane (5 mL) was added to the mixture. After refluxing for 3 h under a nitrogen atmosphere, the reaction

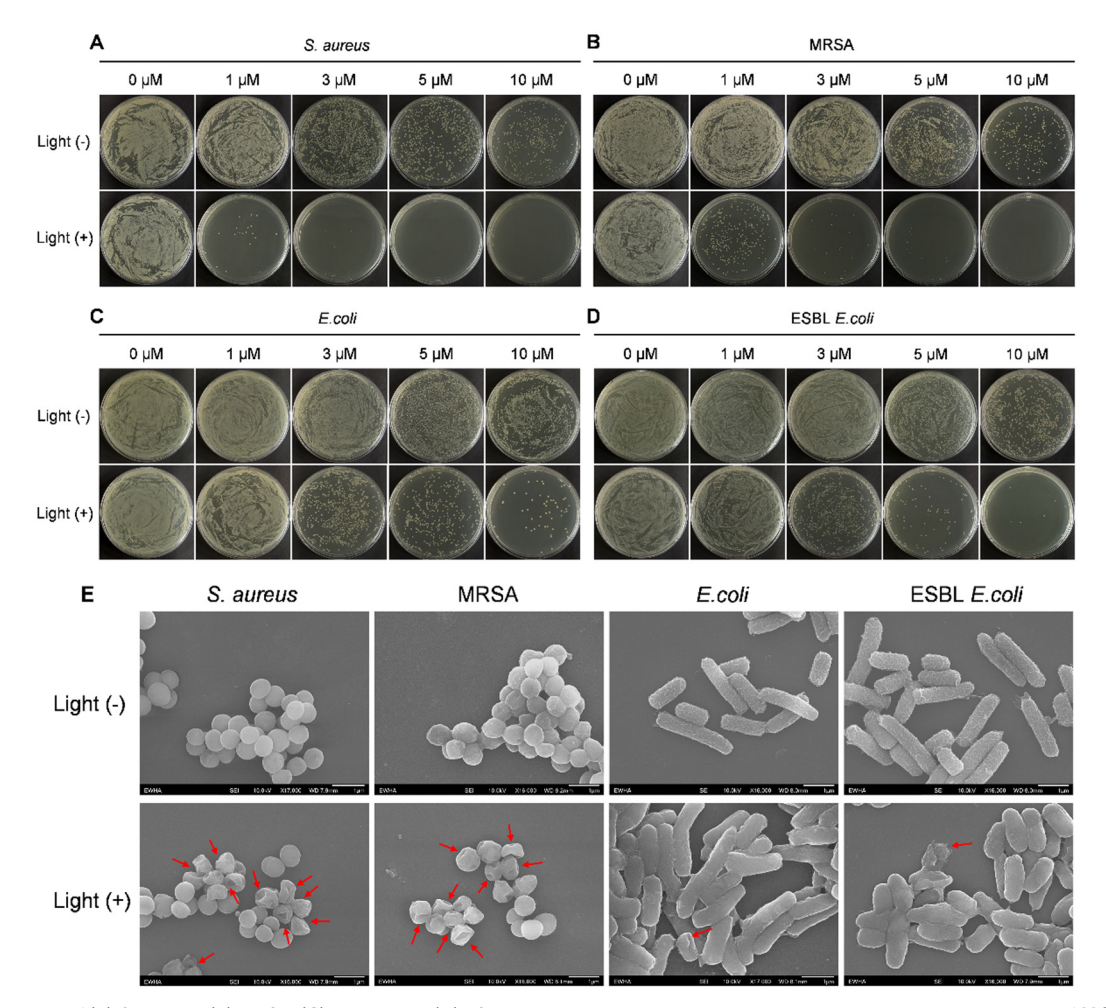


Fig. 6 Photographs of (A) *S. aureus*, (B) MRSA, (C) *E. coli*, and (D) ESBL *E. coli* on LB agar plates treated with various concentrations of **MCQ-1** (0, 1, 3, 5, and 10 μ M) under dark and white LED irradiation (50 mW cm⁻², 10 min). (E) SEM images of *S. aureus*, MRSA, *E. coli*, and ESBL *E. coli* treated with **MCQ-1** (3 μ M) under dark and white LED irradiation (50 mW cm⁻², 10 min).

mixture was cooled to room temperature, then poured into ice water, quenched with aqueous ammonia, and extracted with dichloromethane. The organic layer was dried over Na₂SO₄, followed by evaporation and purification by column chromatography using a n-hexane/ethyl acetate mixture (2:1, v/v) as the eluent to obtain compound 2 in 93.5% yield. ¹H NMR (300 MHz, chloroform-d) δ 10.09 (s, 1H), 8.60 (s, 1H), 8.15 (d, 1H), 8.0 (dd, 1H), 7.57–7.51 (m, 3H), 7.33 (dd, 1H), 4.35 (t, 2H), 3.68 (t, 4H), 2.35 (m, 6H), 1.94 (tt, 2H), 1.57 (tt, 2H).

Synthesis of MCQ-1

Compound 2 (0.286 g, 0.85 mmol, 1 eq) and 1,4-dimethylquinolin-1-ium iodide (0.242 g, 0.85 mmol, 1 eq) were dissolved in 20 mL of anhydrous ethanol. Three drops of piperidine were added as a catalyst. The mixture was refluxed overnight under a nitrogen atmosphere and then cooled to room temperature. After removing the solvent by evaporation, the crude product was purified by column chromatography using a dichloromethane/methanol mixture (30:1, v/v) as the eluent, to obtain **MCQ-1** as a red solid in 50.7% yield. 1 H NMR (300 MHz, DMSO- 2 d₀) δ 9.29 (d, 1H), 9.14 (d, 1H), 8.88 (s, 1H), 8.51–8.24 (m, 6H), 8.09 (m, 2H), 7.75 (dd, 2H),

7.54 (t, 1H), 7.31 (t, 1H), 4.51 (s, 3H), 3.52 (4H), 3.34 (2H), 2.27 (6H), 1.83 (2H), 1.49 (2H). 13 C NMR (125 MHz, DMSO- d_6) δ 153.54, 148.05, 145.39, 142.27, 141.16, 139.32, 135.39, 129.47, 127.20, 126.61, 123.27, 122.70, 122.39, 120.31, 116.69, 115.61, 110.58, 110.56, 44.94, 42.82, 26.66. ESI-HRMS $[C_{32}H_{34}N_3O]^+$, calcd: 476.2702, found $[M]^+$: 476.2702.

Spectral analysis

A 1 mM stock solution of **MCQ-1** was prepared by dissolving it in DMSO. The stock solution was then diluted with various solvents (10 μ M, 2 mL), followed by measuring the UV-vis absorption and fluorescence emission spectra. For fluorescence measurements at different pH levels, the **MCQ-1** stock solution (1 mM) was diluted to 10 μ M (2 mL) in ACN/PBS aqueous solution (5:95, v/v). To adjust the pH values for each measurement, NaOH and HCl solutions were used to control the pH of the PBS medium (pH 7.4).

ROS detection

DCFH-DA and HPF were used as fluorescent probes to detect total ROS and hydroxyl radical (*OH) generation, respectively.

A PBS solution (2 mL) containing the detection probe (25 μM) and MCQ-1 (10 µM) was prepared in a cuvette. The cuvette was then exposed to white LED light (50 mW cm⁻²) for 10 s at a time, and fluorescence was measured immediately after each exposure, continuing for a total of 90 s. Solutions containing only DCFH-DA and HPF were used as controls.

Cell culture

HeLa cell samples, obtained from the Korean Cell Line Bank (Seoul, Korea), were cultured in minimum essential medium (MEM) with 100 U mL⁻¹ penicillin, 100 U mL⁻¹ streptomycin, and 10% fetal bovine serum (FBS). The cells were incubated at 37 °C in a 5% CO₂ atmosphere.

Cell viability tests

The cultured cells were seeded in a 96-well plate. After overnight incubation, the medium was removed, and the cells were treated with different concentrations of MCQ-1 (0-20 µM), followed by incubation for another 24 h. Next, an MTT solution (5 mg mL⁻¹) was added before incubating for an additional 4 h. Formazan crystals were dissolved using 100 µL of DMSO, and the absorbance was measured using a Spectramax Microwell plate reader.

Colocalization imaging

HeLa cells were seeded in 35-mm glass-bottom dishes at a density of 3×10^5 cells per dish. After overnight incubation, the cells were co-stained with MCQ-1 (5 µM) for 30 min and BioTracker 405 Blue Mitochondria Dye (Merck) or LysoTracker Deep Red (Thermo Fisher Scientific) for 10 min. The dishes were then washed with DPBS, and confocal fluorescence images were obtained using an Olympus Fluoview 3000 microscope.

Bacterial culture

Antibacterial tests were conducted using Gram-positive bacteria such as S. aureus (25923) and MRSA (CCRAM 3696), as well as Gram-negative bacteria including E. coli (ATCC 43894) and ESBL E. coli (ATCC BAA-198). The bacteria were first grown on LB agar plates overnight; then, 3-5 colonies from each plate were transferred to 4 mL of LB broth culture and incubated for several hours at 37 °C with shaking at 200 rpm. The optical density (OD) of the bacterial solution at 600 nm was adjusted to 1.0 to standardize the bacterial concentration, ensuring consistent values across the experiments.

Confocal fluorescence imaging

1 mL of bacterial culture was centrifuged at 5000 rpm to obtain a bacterial pellet, which was then washed three times with PBS. The pellet was treated with MCQ-1 (1 µM) in PBS (1 mL) and incubated for 0, 30, and 60 min, respectively. The bacterial solution was centrifuged again, and the pellet was resuspended in an appropriate amount of PBS. Finally, the suspension was placed on a glass microscope slide, and fluorescence images were obtained using an Olympus Fluoview 1200 microscope.

Antibacterial PDT effects

For antibacterial experiments, 1 mL of bacterial culture adjusted to an OD of 1.0 was centrifuged at 5000 rpm to obtain a bacterial pellet. The latter was washed three times with PBS, followed by the addition of 1 mL of PBS to prepare the bacterial stock solution. Next, 100 µL of the bacterial stock solution was mixed with various concentrations of MCQ-1 (0, 1, 3, 5, and 10 μM) in 1 mL of PBS solution, and the resulting mixture was incubated at 37 °C with shaking at 200 rpm for 2 h. After incubation, 200 μL of each sample was exposed to white LED light (50 mW cm⁻²) for 10 min. The irradiated solutions were then diluted 10 times with PBS, and 200 µL of each diluted solution was spread on LB agar plates. Finally, the plates were incubated at 37 °C overnight.

SEM detection

The bacterial culture was centrifuged at 5000 rpm, and the bacterial precipitate was washed three times with PBS. The obtained product was treated with MCQ-1 (3 µM) in PBS (1 mL) and incubated for 2 h. Each sample was irradiated with white LED light (50 mW cm $^{-2}$) for 10 min, then centrifuged and fixed with 2% paraformaldehyde, and sequentially dehydrated using ethanol solutions of increasing concentrations (30%, 50%, 75%, 85%, 95%, and 100%). Finally, the dehydrated bacterial samples, placed on a silicon wafer, were allowed to dry and then examined using SEM.

Theoretical methods

All calculations were performed with the ORCA 6.0.1 software package³⁵ at the CAM-B3LYP/TZVP level of theory.³⁶ Solvent effects were included using the SMD solvation model, with water as the solvent.³⁷ The DFT-D3 dispersion correction was applied throughout the calculations. Electron-hole analysis was performed using the Multiwfn 3.8 package.³⁸

Conclusions

Photoactivated fluorescent probes capable of inducing lysosomal dysfunction and mitochondrial damage in situ are highly desirable, owing to advantages such as light-controlled imaging with high spatial resolution and the enhanced therapeutic effects of dual-organelle disruption. In this study, we developed and characterized a novel dual-targeting type I PS, MCQ-1, capable of localizing both mitochondria and lysosomes in cancer cells. This compound exhibited favorable photophysical properties, including a large Stokes shift and strong red fluorescence, enabling effective cellular imaging. Moreover, MCQ-1 showed a strong pH-dependent fluorescence behavior, with enhanced emission in acidic environments, and maintained a sufficiently strong signal under physiological conditions, highlighting its applicability in biological systems.

Upon white light irradiation, MCQ-1 efficiently generated ROS, including hydroxyl radicals (OH), via a type I photodynamic mechanism. Confocal imaging confirmed its dualtargeting capability, with high colocalization to mitochondria and lysosomes. Importantly, MCQ-1 showed low cytotoxicity in the dark but high phototoxicity under light exposure, highlighting its potential as a safe and effective PDT agent.

Furthermore, MCQ-1 exhibited selective antibacterial activity against Gram-positive bacteria, including MRSA, through a light-triggered PDT process. This compound also enabled rapid and selective staining of Gram-positive bacteria and induced significant morphological damage upon irradiation. In contrast, Gram-negative bacteria showed limited susceptibility to MCQ-1, indicating that the observed specificity is likely driven by bacterial cell wall composition.

Taken together, these results demonstrate that MCQ-1 is a promising dual-functional photosensitizer that combines organelle-targeted cancer therapy and selective antimicrobial activity. Its dual-targeting ability, efficient ROS generation, and biocompatibility make it a valuable candidate for further applications in both oncology and infectious disease treatment.

Author contributions

Chaewoon Cho: synthesis, investigation, and writing - original draft. K. M. K. Swamy: conceptualization and synthesis. Bingqing Sun: theoretical calculations and writing - review and editing. Gyoungmi Kim: cell culture and confocal fluorescence imaging. Lei Liu: theoretical calculations and writing - review and editing. Won Jun Jang: writing - review and editing. Juyoung Yoon: conceptualization and writing - original draft and editing.

Conflicts of interest

There are no conflicts to declare.

Data availability

The data supporting this article have been included as part of the ESI.†

Acknowledgements

This work was supported by the National Research Foundation (NRF), funded by the Korean government (MSIT) (RS-2023-00217701). K. M. K. Swamy thanks the Brain Pool program, funded by the Ministry of Science and ICT through the National Research Foundation of Korea (RS-2023-00304224). This research was also supported by the Natural Science Foundation of the Anhui Higher Education Institutions of China (Grant No. gxgwfx2021037 and gxgwfx2022027) and the Foundation of the Anhui Science and Technology University (Grant No. 2021zrzd15). NMR measurements were performed using the 300 MHz spectrometer at the National Research Facilities and Equipment Center (NanoBioEnergy Materials Center) of Ewha Womans University.

Notes and references

1 X.-X. Lu, C. Xue, J.-H. Dong, Y.-Z. Zhang and F. Gao, J. Mater. Chem. B, 2024, 12, 3209-3225.

- 2 X. Lyu, J. Yu, L. Zhang, Y. Zhao, Z. Qiu, Y. Chen, Z. Zhao and B. Z. Tang, J. Mater. Chem. B, 2023, 11, 5953-5975.
- 3 Y.-Y. Zhao, H. Kim, V.-N. Nguyen, S. Jang, W. J. Jang and J. Yoon, Coord. Chem. Rev., 2024, 501, 215560.
- 4 T. Xiong, Y. Chen, Q. Peng, X. Zhou, M. Li, S. Lu, X. Chen, J. Fan, L. Wang and X. Peng, *Adv. Mater.*, 2025, **37**, 2410992.
- 5 Y.-Y. Zhao, X. Zhang, Y. Xu, Z. Chen, B. Hwang, H. Kim, H. Liu, X. Li and J. Yoon, Angew. Chem., Int. Ed., 2024, 63, e202411514.
- 6 B. Lu, L. Wang, H. Tang and D. Cao, J. Mater. Chem. B, 2023, 11, 4600-4618.
- 7 S. Zeng, J. Wang, H. Kang, H. Li, X. Peng and J. Yoon, Angew. Chem., Int. Ed., 2025, 64, e202417899.
- 8 R. Wang, X. Li and J. Yoon, ACS Appl. Mater. Interfaces, 2021, **13**, 19543-19571.
- 9 N. Sun, R. J. Youle and T. Finkel, Mol. Cell, 2016, 61, 654-666.
- 10 H. Li, H. Kim, C. Zhang, S. Zeng, Q. Chen, L. Jia, J. Wang, X. Peng and J. Yoon, Coord. Chem. Rev., 2022, 473, 214818.
- 11 Q. Ding, X. Wang, Y. Luo, X. Leng, X. Li, M. Gu and J. S. Kim, Coord. Chem. Rev., 2024, 508, 215772.
- 12 E. R. H. Walter, P. K.-K. Leung, L. C.-C. Lee, K. K.-W. Lo and N. J. Long, J. Mater. Chem. B, 2024, 12, 10409-10415.
- 13 H. Li, Y. Lu, J. Chung, J. Han, H. Kim, Q. Yao, G. Kim, X. Wu, S. Long, X. Peng and J. Yoon, Chem. Sci., 2021, 12, 10522-10531.
- 14 C. Kim, H. Kim, J. Jo, S. Kim, A. M. Bongo, H.-J. Kim and J. Yang, ACS Appl. Bio Mater., 2024, 7, 8294–8304.
- 15 W. Li, S. Yin, Y. Shen, H. Li, L. Yuan and X. Zhang, J. Am. Chem. Soc., 2023, 145, 3736-3747.
- 16 Z. Zhou, S. Li, X. Ding, K. Zhang, J. Zhou and X. Zhou, ACS Appl. Bio Mater., 2025, 8, 3464-3472.
- 17 C. Su, P. Xing, J. Zhang, X. Ma, X. Wu, M. Zhu, X. Zhang, H. Du, Y. Bian and J. Jiang, Dyes Pigm., 2024, 222, 111861.
- 18 H. Wu, S. Lee, H. Kim, S. Hong, T. Kim, S. Yeo, W. K. Lee and I. Yoon, Dyes Pigm., 2024, 224, 112039.
- 19 K. Xue, P. Zhang, Y. Zhao, S. Sun, Y. Li, J. Liang and Z. Qi, Dyes Pigm., 2023, 217, 111442.
- 20 Z. Liu, Z. Tang, Y. Yin, M. Wan, J. Zhan and L. Ren, Adv. Healthcare Mater., 2025, 2403954.
- 21 X. Wen, Z. Shi, Y. Huang and Z. Fan, New J. Chem., 2024, 48, 19136-19143.
- 22 F. F. Li, J. G. Collins and F. R. Keene, Chem. Soc. Rev., 2015, 44, 2529-2542.
- 23 B. Hu, C. Owh, P. L. Chee, W. R. Leow, X. Liu, Y. L. Wu, P. Guo, X. J. Loh and X. Chen, Chem. Soc. Rev., 2018, 47, 6917-6929.
- 24 P. C. Ray, S. A. Khan, A. K. Singh, D. Senapati and Z. Fan, Chem. Soc. Rev., 2012, 41, 3193-3209.
- 25 H. Kim, Y. R. Lee, H. Jeong, J. Lee, X. Wu, H. Li and J. Yoon, Smart Molecules, 2023, 1, e20220010.
- 26 W. Zhou, Q. Qiao, Y. Tao, C. Duan, J. Li, X. Fang, N. Xu, J. Chen, W. Liu, L. Miao and Z. Xu, Sens. Actuators, B, 2024, 410, 135691.
- 27 J. H. Liu, X. L. Chen, H. M. Yang, Y. R. Yin, A. Kurniawan and Ch. H. Zhou, J. Mater. Chem. B, 2024, 12, 6874-6885.
- 28 X. Wu, M. Yang, J. S. Kim, R. Wang, G. Kim, J. Ha, H. Kim, Y. Cho, K. T. Nam and J. Yoon, Angew. Chem., Int. Ed., 2022, 61, e202200808.

Paper

- 29 Ferdinandus, C. Joo, D. Kai and C.-L. Ken Lee, J. Mater. Chem. B, 2023, 11, 5748-5751.
- 30 B. Maji, K. Kumar, M. Kaulage, K. Muniyappa and S. Bhattacharya, J. Med. Chem., 2014, 57, 6973-6988.
- 31 J. Luo, G. Song, X. Xing, S. Shen, Y. Ge and X. Cao, New J. Chem., 2017, 41, 3986-3990.
- 32 Z. Fang, F. Pei, Z. Chao, L. Hui, Q. Ying and W. Xiang, Indian J. Chem., 2016, 55B(6), 713-717.
- 33 Q. Wan, R. Zhang, Z. Zhuang, Y. Li, Y. Huang, Z. Wang, W. Zhang, J. Hou and B. Z. Tang, Adv. Funct. Mater., 2020, 30, 2002057.
- 34 Z. Liu, Q. Wang, W. Qiu, Y. Lyu, Z. Zhu, X. Zhao and W. H. Zhu, Chem. Sci., 2022, 13, 3599-3608.
- 35 F. Neese, The ORCA program system, WIREs Comput. Mol. Sci., 2012, 2, 73-78.
- 36 A. V. Marenich, C. J. Cramer and D. G. Truhlar, J. Phys. Chem. B, 2009, 113, 6378-6396.
- 37 S. Grimme, J. Antony, S. Ehrlich and H. Krieg, J. Chem. Phys., 2010, 132, 154104.
- 38 T. Lu and W. F. Chen, J. Comput. Chem., 2012, 33, 580-592.
- 39 X. Kang, Z. Du, S. Yang, M. Liang, Q. Liu and J. Qi, Smart Molecules, 2024, 2, e20240033.